



CHORUS

This is the accepted manuscript made available via CHORUS. The article has been published as:

Ordering mechanism and quantum anomalous Hall effect of magnetically doped topological insulators

Jeongwoo Kim, Seung-Hoon Jhi, A. H. MacDonald, and Ruqian Wu

Phys. Rev. B **96**, 140410 — Published 25 October 2017

DOI: [10.1103/PhysRevB.96.140410](https://doi.org/10.1103/PhysRevB.96.140410)

Ordering Mechanism and Quantum Anomalous Hall Effect of Magnetically Doped Topological Insulators

Jeongwoo Kim¹, Seung-Hoon Jhi², A.H. MacDonald³, and Ruqian Wu^{1*}

¹*Department of Physics and Astronomy, University of California, Irvine, California 92697, USA*

²*Department of Physics, Pohang University of Science and Technology, Pohang 790-784, Republic of Korea*

³*Department of Physics, University of Texas at Austin, Austin, Texas 78712, USA*

Abstract:

We investigate magnetic ordering and the quantum anomalous Hall effect (QAHE) in Cr-doped topological insulators (TIs) using systematic first-principles calculations, explaining the mechanism responsible for ferromagnetic order and the reason why Sb_2Te_3 is a better QAHE host than Bi_2Se_3 or Bi_2Te_3 . We conclude that these magnetic topological insulators have relatively long-range exchange interactions within quintuple layers, and weak interactions between quintuple layers. Our analyses for the spin splitting of the topological surface states suggest that the temperature at which the QAHE occurs in these materials can be significantly enhanced by Mo-Cr co-doping.

PACS numbers: 75.50.Pp, 73.20.At, 73.43.Cd

The demonstration of a robust quantum anomalous Hall effect (QAHE) in magnetically doped topological insulators (TIs), has attracted great interest [1-3]. Bi_2Se_3 (BS), Bi_2Te_3 (BT), and Sb_2Te_3 (ST) are prototypical three-dimensional TIs with sizeable topologically nontrivial bulk band gaps produced by a combination of band inversion and strong spin-orbit coupling (SOC). These materials provide a potential platform for fundamental studies demonstrating novel phenomena thought to be associated with topological bands, including magnetic monopoles [4], axion dynamics [5], and Majorana fermions [6]. The protected topological surface states (TSSs) of TIs have strong spin-momentum locking [7] and manifest a robust QAHE when the TIs are magnetized by magnetic dopants [1, 8, 9]. One puzzling issue in this regard is that the QAHE has so far been observed only at extremely low temperatures, *e.g.*, below ≈ 30 mK in Cr- or V-doped $(\text{Bi,Sb})_2\text{Te}_3$ (BST) [2, 3, 10-12]. Extensive effort has been dedicated to enhancing the magnetic ordering among dopants [13, 14] and hence the T_c of magnetic TIs [15, 16]. Nevertheless, it appears that the characteristic temperature for the realization of the QAHE is not greatly improved, and that the QAHE is sometimes absent even in samples that show clear hysteresis loops. To address the challenge of achieving a QAHE at a reasonably high temperature, it is crucial to disentangle the factors that play in governing the magnetic order and topological properties of these materials.

In previous work no consensus has been reached regarding the ordering mechanism of magnetic dopants in TIs. Taking Cr-doped TIs as an example, it was found that although BS, BT, and ST are very similar in many respects, Cr atoms produce clear ferromagnetic (FM) order in BT and ST, whereas they do not yield a clear hysteresis loop in BS [17-21]. It is however established that when it occurs magnetic ordering in TI is rather independent of carrier density [21]. Recently, superparamagnetic ordering between magnetic domains has

also been observed in Cr-doped TIs, through transport measurements [10] and scanning magnetic images [23]. These observations cannot be satisfactorily explained either by normal van Vleck type ferromagnetism [1] or by a Ruderman-Kittel-Kasuya-Yosida (RKKY) type exchange mechanism [20, 22]. It is therefore imperative to address the ordering mechanism, particularly the influence of the TSSs that are often thought to play a role in magnetic TIs.

In this Letter, we examine the electronic structure of Cr-doped TIs with a variety of different structural and magnetic configurations, using first-principles density-functional theory (DFT) calculations. The dependences of TSS properties and magnetic ordering on the change of doping concentration, the arrangement of dopants, and the strength of SOC are carefully examined. Our study explains the magnetic ordering mechanism and answers other questions that have been puzzling, *e.g.*, 1) Why does Cr-doped BS have no long-range ferromagnetism? 2) Why is a small amount of Bi needed for the observation of the QAHE in Cr-doped ST? Furthermore, we suggest a pragmatic way to realize the QAHE at a higher temperature, namely by using Mo co-doping.

Our DFT calculations use the projected augmented plane-wave method [24, 25] as implemented in the Vienna *ab initio* simulation package (VASP) [26]. The generalized gradient approximation is used for the DFT exchange-correlation potential [27], along with the van der Waals corrections [28]. SOC is included in the self-consistency loops. The energy cutoff for the plane-wave-basis expansion is chosen to be 300 eV. Surface calculations are performed using 5 quintuple-layer (QL) slabs separated by ~ 15 Å of vacuum, and bulk simulations are done with a supercell containing 240 atoms. We employ a $4 \times 4 \times 1$ \mathbf{k} -point grid to sample the Brillouin zone and the convergence is carefully examined (Fig. S1 [29]). The positions of all atoms are fully relaxed until total energies are converged to better than 0.1 meV per formula unit. We consider only Cr atoms substituted on the energetically favored Sb

(or Bi) sites as shown in Fig. S2 [29,30]. In all cases, the substituted Cr atoms have a stable +3 oxidation state with three occupied t_{2g} orbitals contributing a $3 \mu_B$ local magnetic moment over a reasonable range of Hubbard- U (Fig. S3 [29]).

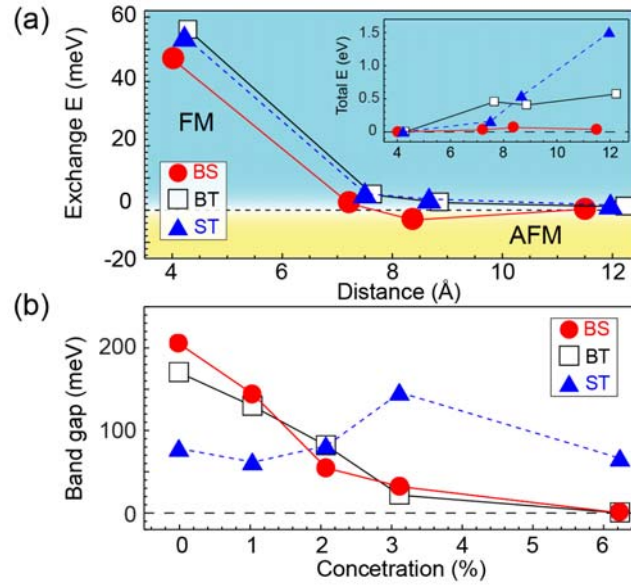


Figure 1 (Color online) (a) Exchange energies as a function of Cr-Cr distance for Bi_2Se_3 (red circles), Bi_2Te_3 (black squares), and Sb_2Te_3 (blue triangles). Positive (negative) values imply lower energy for parallel (opposite) Cr spin orientations. The inset shows total energies versus Cr-Cr distance in TIs containing two Cr dopants. The zero energy is set to the value for the shortest Cr-Cr distance. (b) Calculated band gaps of Cr-doped TIs as a function of Cr concentration with Cr atoms.

We first address the energetically preferred spatial distribution of Cr atoms by varying the inter-Cr distance in bulk BS, BT and ST systems with two magnetic dopants in the same cation plane. The behavior of Cr dopants in BS is very different from that in BT and ST [Fig. 1(a), inset]. The magnetic dopants prefer to stay close to each other in ST and BT. In BS, the total energy does not show a drastic increase with $d_{\text{Cr-Cr}}$ and even decreases beyond $d_{\text{Cr-Cr}} \sim 11 \text{ \AA}$. We attribute this feature to the different sizes of Se and Te. When Cr atoms are

introduced into cation (Bi or Sb) sites, anions (Te or Se) relax toward the Cr atoms. The relaxation is larger for Se atoms due to their smaller atomic radius. The energetic preference for larger distances between Cr atoms in the BS case likely follows from a preference for weakened structural stress. Se and Te atoms also produce different behaviors in the exchange coupling dependence of $d_{\text{Cr-Cr}}$. In Fig. 1(a), the energy differences between the parallel spin (FM) and opposite spin (AFM) magnetic dopant configurations, indicates that ST and BT exchange interactions are ferromagnetic out to $d_{\text{Cr-Cr}} = 12 \text{ \AA}$, whereas those of BS turn antiferromagnetic when $d_{\text{Cr-Cr}}$ becomes larger than 7.5 \AA . Even for the closest Cr dopants in BS, AFM interactions can occur, depending on the Cr configuration as shown in Fig. S4 [29]. We note that the experimental magnetic moment of BS is less than 70% of the complete spin-polarization value, suggesting that some exchange interactions are AFM [31]. These results suggest, in agreement with experimental observations, [18, 19, 31] that the total exchange energy of Cr dopants in BT and ST is likely to be minimized when all spins are parallel, whereas the ground magnetic configuration of BS is likely to be more complicated and more sensitive to the spatial distribution of Cr dopants.

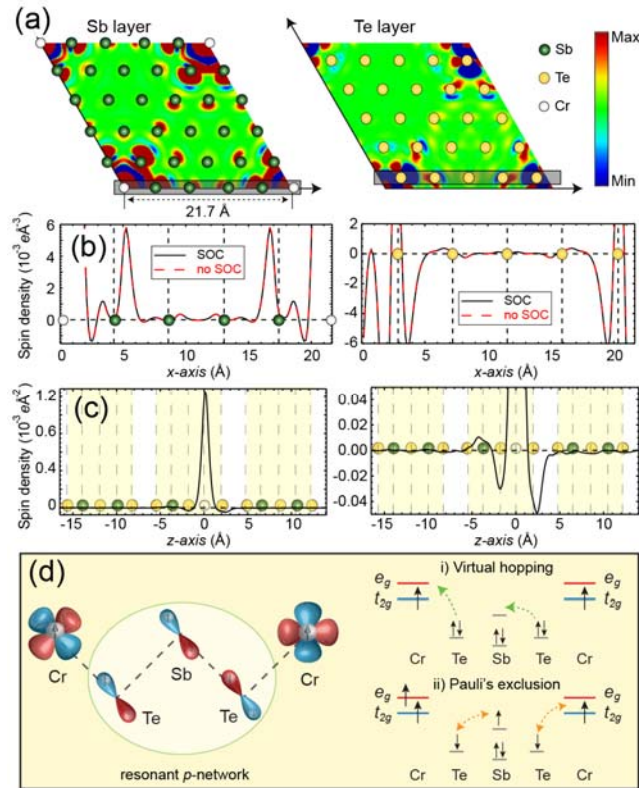


Figure 2 (Color online) (a) The spin density of a Sb (Green) layer with Cr (white) dopants and of a Te (yellow) layer in Cr-doped Sb₂Te₃. The color scale covers the range from -4.0×10^{-4} to 4.0×10^{-4} e/Å³. (b) Line profiles corresponding to the shaded regions of Sb (left panel) and Te layer (right panel), respectively. (c) The layer averaged spin density is plotted along the z-axis. The Cr dopant is located at the Sb layer set to zero and the regions shaded yellow represent QLs. When segregated on the Sb sublattice, Cr local moments transfer parallel spins from Te to Sb sites and opposite spin from Sb to Te, favoring ferromagnetic local moment alignment. (d) Schematic drawings of orbital hybridization and spin configuration for Cr-doped Sb₂Te₃. The ferromagnetic ordering between Cr dopants is mediated through the resonant p-network.

Regarding the ordering mechanism in ST, our most important observation is that the FM order survives when SOC is turned off, as illustrated Fig. S5 [29]. The magnetic order of

Cr-doped ST is not governed by a van Vleck type mechanism that relies on nontrivial band topology (ST is a trivial insulator when SOC is neglected.) [1]. Since ST remains insulating as long as the concentration of Cr atoms is less than $\sim 10\%$, as displayed in Figs. 1(b) and S6 [29], the FM ordering of Cr-doped ST is not due to bulk RKKY interactions either. Equally surprising, our model calculations for two Cr dopants in a 5-QL ST film indicate that the magnetic moments and the exchange energies change only weakly when we move the two Cr dopants from the surface QL to the interior region (Fig. S7 [29]), even though the TSSs have substantially different weights in these QLs, demonstrating that surface states do not have an important role. According to our DFT calculations, the ordering mechanism is instead related to the spatial segregation of Cr dopants on Sb sites, and to contributions to the charge polarizability of the Sb_2Te_3 lattice from orbitals far from the topological gap. This mechanism is easiest to understand in the limit in which SOC is neglected so that the charge and spin-susceptibilities of the host crystal are identical. When the interactions between Cr local moments and itinerant orbitals are treated perturbatively, the dependence of energy on Cr spin-orientation is proportional to the cation sublattice spin-response function. In diluted moment systems, robust order depends on response that is insensitive to the spatial distribution of magnetic dopants, and therefore related in the perturbative limit to $q=0$ response functions. In insulators, the total charge (and in the absence of SOC also the total spin) response function vanishes at $q=0$. Sublattice-projected response function need not vanish however. Fig. 2 (a) shows that the spin density response to Cr substitution on an Sb site polarizes the p -electron bonding network and strongly favors parallel alignment of Cr spins. The exchange interaction is not strongly affected by SOC [Fig. 2(b)]. The small amplitude of the averaged spin density in other QLs away from the one with Cr dopant in Fig. 2(c) implies relatively weak exchange interactions between different QLs. Since

chalcogenides have a long-range resonant p -bonding [32] network within each QL, the induced spin polarization can spread widely [Fig. 2(d)]. Both Cr- e_g and Sb- p orbitals form σ -type directional bonds with Te and the network of bonds effectively mediate magnetic coupling among Cr atoms. The mechanism is similar in part to that responsible for the ferromagnetism of sublattice-segregated hydrogen local moments in graphene [33].

Aside from the ferromagnetic ordering of Cr dopants in these TIs, two other prerequisites for the observation of QAHE are that (1) the bulk TI retains its insulating nature in the presence of Cr dopants; and (2) the TSS is magnetized and has a gap. To this end, we investigate changes in the band structures of the three TIs, particularly changes of their band gaps, as we increase the concentration of Cr dopants [34]. The results in Fig. 1(c) show that BS and BT become metallic by 6% Cr doping whereas ST has a gap until $\sim 10\%$ Cr doping. This implies that, even disregarding the issue of weak FM ordering in BS, the QAHE is unlikely to be observed in Cr-doped BS and BT because bulk conduction overwhelms TSS conduction.

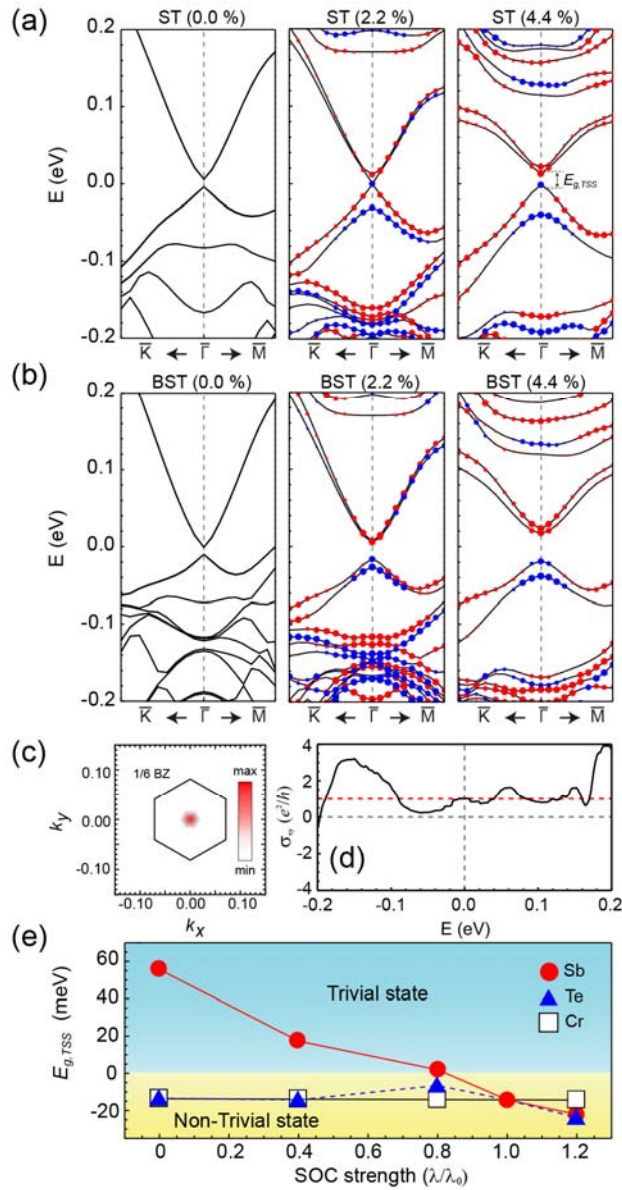


Figure 3 (Color online) Calculated band structures of Cr-doped (a) Sb_2Te_3 and (b) $(Bi,Sb)_2Te_3$ in a 5QL-thick film. Cr dopants are placed in the outermost QL and the Cr concentration is given at the top of each panel. Spin up (down) states are marked by red (blue) dots. (c) and (d) show the calculated Berry curvature of the valence bands in the Brillouin zone and the corresponding anomalous Hall conductivity (σ_{xy}) of a Cr-doped Sb_2Te_3 film. Red dashed line in (d) marks the Hall conductivity with a Chern number of 1. (e) The variation of

the TSS gap ($E_{g,TSS}$) upon the change of the SOC strength in Cr-doped Sb_2Te_3 (4.4%). The atomic SOC constant of Sb (red circles), Te (blue triangles) or Cr (white squares) is selectively changed from 0 to 1.2 in relative to the native value while the rest is fixed to the native value.

Cr-doped ST appears to be the only candidate for the realization of QAHE among the three TIs and hence our slab calculations focus on this material. For these calculations Cr dopants are distributed in the outermost QL of ST where the TSSs have the largest weight [35] to maximize their influence on the TSSs. The band structure of a 5-QL Sb_2Te_3 slab exhibits a small band gap ($E_{g,TSS} \sim 10$ meV) at the Γ point due to intersurface hybridization. When 2.2% of Sb atoms are replaced by Cr, the TSSs become magnetized and the gap closes [Fig. 3(a)]. At higher Cr concentrations (4.4%), the gap reopens and the QAHE is established by inverting bands associated with two different spin states. We confirm that the TSSs of Cr-doped ST have nonzero Berry curvature and quantized Hall conductivity with Chern number 1 [Figs. 3(c) and (d)], indicative of the QAH phase. Furthermore, calculations for a semi-infinite boundary [36] reconfirm that Cr-doped ST has chiral 1D conduction channels on its sidewalls, as shown in Fig. S8 [29]. We find, in agreement with experiment [2, 10-12], that introduction of Bi atoms into Sb expedites the transition to a QAH state. Due to the similarity between Bi and Sb in electronic configuration, Bi doping up to 11% does not dramatically change in electronic structure of ST around the Fermi level, as shown in Fig. 3(b). Nevertheless, when both Bi and Cr are dispersed into ST, the transition to a QAH state has already occurred at 2.2% Cr doping [Fig. 3(b)] and the TSS gaps tend to be larger.

To reveal the effect of SOC of cations in TI on band inversion in Cr-doped (4.4%) Sb_2Te_3 , we vary the SOC strength of each atom from 0 to 1.2 times its native value and trace the 2D bands of the slab geometry near the Γ point [Fig. 3(e)]. We find that the variation of

the SOC constant of Cr does not change the band order of the Dirac states. The band gap of Cr-doped Sb_2Te_3 is more sensitive to the SOC strength of Sb than that of Te in spite of its smaller atomic number. The close correlation between the SOC strength of the cation and the TSS band gap shown in Fig. 3(e) explains why the introduction of Bi with a strong SOC facilitates the observation of QAHE in experiment. Although unimportant for magnetic order, SOC is essential to establish the QAHE.

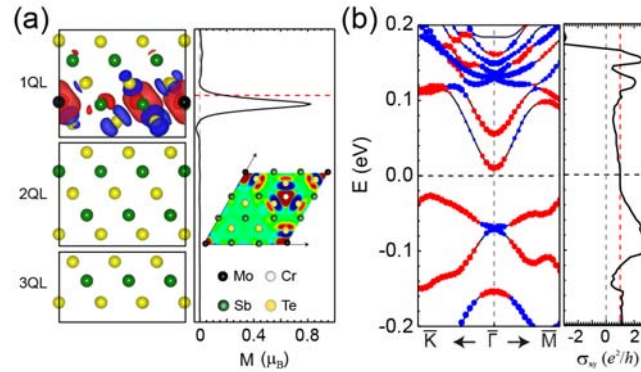


Figure 4 (Color online) (a) The spin density and its planar average of 5 QL Sb_2Te_3 with Mo-Cr co-doping. The inset is the top-view in the plane near the impurity (at the position marked by the red dashed line). Red (blue) regions mean positive (negative) spin densities. (b) Calculated band structure and anomalous Hall conductivity (σ_{xy}) of 4 QL Sb_2Te_3 with Mo-Cr co-doping in the outermost QL. Bands with spin up (down) states are marked by red (blue) dots. Red dashed line in (b) marks the Hall conductivity with a Chern number of 1.

Contrary to intuitive expectations, the Γ point spin splitting of the Dirac cone does not vary strongly with Cr concentration as shown in Fig. S9 [29]. The small size of this spin splitting is the main reason why the QAHE is observed only at very low temperature (< 1 K) in BST, well below the Curie temperature, which can be as high as 15 K [2]. To mitigate this problem, co-doping can be a solution as was recently discussed by Qi *et al.* for codoping vanadium and iodine in ST [37]. Here, we propose Mo co-doping along with Cr as a way to

simultaneously increase the spin splitting and SOC strength of TSSs as Mo has a tendency of being magnetic in an environment with weak interaction. Our calculations indicate that Mo has a local magnetic moment of $2.0 \mu_B$ in ST and BST, and favors FM ordering with Cr as shown in Fig. S10 [29]. The spin density distribution shown in Fig. 4(a) indicates that Mo and Cr induce magnetization over a rather large range in the Sb plane, and that Te has the opposite spin polarization compared to that of Sb and the dopants. The band structure of Fig. 4(b) obviously shows that the conduction and valence bands become inverted in Mo-Cr co-doped ST. It is also significant to see that Mo-Cr co-doping (6.25% each) increases the inverted band gap to 36 meV in Fig. 4(b), much larger than 16 meV without Mo (12.5% Cr) in Sb_2Te_3 as shown in Fig. S8 [29]. In addition, Mo-Cr co-doped Sb_2Te_3 exhibits +1 Chern number near the Fermi level [Fig. 4(b)]. This suggests a new possibility of the realizing QAHE at a higher temperature. We note that, even in the dilute doping regime, the inverted band gap is enhanced from 14 meV (4.4% Cr) [Fig. 3(a)] to 57 meV (2.2% each) (Fig. S11 [29]). Therefore, even a small amount of Mo doping can allow the quantized Hall conductivity to be observed more easily. We also tested other transition metals as co-dopants but found that they either become nonmagnetic or mess up the bands of TSSs near the Fermi level (Fig. S12 [29]). It is worthwhile to point out that we only need to introduce magnetic impurities in the surface region of TI for the realization of QAHE. Therefore, the technical difficulty for incorporating Mo that has a high melting point can be circumvented by using surface doping techniques such as ion implementation.

In summary, we studied magnetic ordering mechanism and the QAHE in Cr-doped TIs through systematic DFT calculations. We conclude that the mechanism of magnetic order involves the entire p -bonding network, making it relatively insensitive to details of electronic structure near the Fermi level, including the presence or absence of spin-orbit coupling and

topologically protected edge states. We also found that BS and BT are unlikely to host a QAHE, either due to the lack of robust FM ordering or rapid reduction in the bulk band gap as Cr dopants are added. Based on the insights obtained through studies of Cr-ST(BST), we propose using Mo and Cr co-doping to enlarge the spin splitting of TSSs of ST and BST so that QAHE may persist to a higher temperature. The understanding of the mechanism of magnetic ordering and of the evolution of TSSs established in this work opens the door for the rational design and optimization of new materials and ultimately for the exploitations of the QAHE.

Work was supported by SHINES, an Energy Frontier Research Center funded by the U.S. Department of Energy, Office of Science, Basic Energy Sciences under Grant No. SC0012670. Calculations were performed on parallel computers at the NERSC. SHJ was supported by the National Research Foundation of Korea through SRC program (Grant No. 2011-0030046). Work in Austin was supported in part by Welch Foundation research grant TBF1473.

References:

- [1] R. Yu, W. Zhang, H.-J. Zhang, S.-C. Zhang, X. Dai, and Z. Fang, *Science* **329**, 61 (2010).
- [2] C.-Z. Chang, J. Zhang, X. Feng, J. Shen, Z. Zhang, M. Guo, K. Li, Y. Ou, P. Wei, L.-L. Wang, Z.-Q. Ji, Y. Feng, S. Ji, X. Chen, J. Jia, X. Dai, Z. Fang, S.-C. Zhang, K. He, Y. Wang, L. Lu, X.-C. Ma, and Q.-K. Xue, *Science* **340**, 167 (2013).
- [3] C.-Z. Chang, W. Zhao, D. Y. Kim, H. Zhang, B. A. Assaf, D. Heiman, S.-C. Zhang, C. Liu, M. H. W. Chan, and J. S. Moodera, *Nat. Mater.* **14**, 473 (2015).
- [4] X.-L. Qi, R. Li, J. Zang, and S.-C. Zhang, *Science* **323**, 1184 (2009).
- [5] R. Li, J. Wang, X.-L. Qi, and S.-C. Zhang, *Nat. Phys.* **6**, 284 (2010).
- [6] L. Fu, and C. L. Kane, *Phys. Rev. Lett.* **100**, 096407 (2008).
- [7] M. Z. Hasan, and C. L. Kane, *Rev. Mod. Phys.* **82**, 3045 (2010).
- [8] H.-Z. Lu, A. Zhao, and S.-Q. Shen, *Phys. Rev. Lett.* **111**, 146802 (2013).
- [9] J. Kim, S.-H. Jhi, and R. Wu, *Nano Lett.* **16**, 6656 (2016).
- [10] A. J. Bestwick, E. J. Fox, X. Kou, L. Pan, K. L. Wang, and D. Goldhaber-Gordon, *Phys. Rev. Lett.* **114**, 187201 (2015).
- [11] Y. Feng, X. Feng, Y. Ou, J. Wang, C. Liu, L. Zhang, D. Zhao, G. Jiang, S.-C. Zhang, K. He, X. Ma, Q.-K. Xue, and Y. Wang, *Phys. Rev. Lett.* **115**, 126801 (2015).
- [12] J. G. Checkelsky, R. Yoshimi, A. Tsukazaki, K. S. Takahashi, Y. Kozuka, J. Falson, M. Kawasaki, and Y. Tokura, *Nat. Phys.* **10**, 731 (2014).
- [13] Z. Zhang, X. Feng, M. Guo, K. Li, J. Zhang, Y. Ou, Y. Feng, L. Wang, X. Chen, K. He, X. Ma, Q. Xue, and Y. Wang, *Nat. Commun.* **5**, 4915 (2014).
- [14] Y. Fan, P. Upadhyaya, X. Kou, M. Lang, S. Takei, Z. Wang, J. Tang, L. He, L.-T. Chang, M. Montazeri, G. Yu, W. Jiang, T. Nie, R. N. Schwartz, Y. Tserkovnyak, and K. L.

Wang, *Nat. Mater.* **13**, 699 (2014).

[15] M. Li, C.-Z. Chang, B. J. Kirby, M. E. Jamer, W. Cui, L. Wu, P. Wei, Y. Zhu, D. Heiman, J. Li, and J. S. Moodera, *Phys. Rev. Lett.* **115**, 087201 (2015).

[16] W. Liu, L. He, Y. Xu, K. Murata, M. C. Onbasli, M. Lang, N. J. Maltby, S. Li, X. Wang, C. A. Ross, P. Bencok, G. van der Laan, R. Zhang, and K. L. Wang, *Nano Lett.* **15**, 764 (2015).

[17] C.-Z. Chang, P. Tang, Y.-L. Wang, X. Feng, K. Li, Z. Zhang, Y. Wang, L.-L. Wang, X. Chen, C. Liu, W. Duan, K. He, X.-C. Ma, and Q.-K. Xue, *Phys. Rev. Lett.* **112**, 056801 (2014).

[18] J. Zhang, C.-Z. Chang, P. Tang, Z. Zhang, X. Feng, K. Li, L.-l. Wang, X. Chen, C. Liu, W. Duan, K. He, Q.-K. Xue, X. Ma, and Y. Wang, *Science* **339**, 1582 (2013).

[19] Z. Zhou, Y.-J. Chien, and C. Uher, *Phys. Rev. B* **74**, 224418 (2006).

[20] C.-Z. Chang, J. Zhang, M. Liu, Z. Zhang, X. Feng, K. Li, L.-L. Wang, X. Chen, X. Dai, Z. Fang, X.-L. Qi, S.-C. Zhang, Y. Wang, K. He, X.-C. Ma, and Q.-K. Xue, *Adv. Mater.* **25**, 1065 (2013).

[21] X. Kou, M. Lang, Y. Fan, Y. Jiang, T. Nie, J. Zhang, W. Jiang, Y. Wang, Y. Yao, L. He, and K. L. Wang, *ACS Nano* **7**, 9205 (2013)..

[22] M. Ye, W. Li, S. Zhu, Y. Takeda, Y. Saitoh, J. Wang, H. Pan, M. Nurmamat, K. Sumida, F. Ji, Z. Liu, H. Yang, Z. Liu, D. Shen, A. Kimura, S. Qiao, and X. Xie, *Nat. Commun.* **6**, 8913 (2015).

[23] E. O. Lachman, A. F. Young, A. Richardella, J. Cuppens, H. R. Naren, Y. Anahory, A. Y. Meltzer, A. Kandala, S. Kempinger, Y. Myasoedov, M. E. Huber, N. Samarth, and E. Zeldov, *Sci. Adv.* **1**, e1500740 (2015).

[24] P. E. Blöchl, *Phys. Rev. B* **50**, 17953 (1994).

- [25] G. Kresse, and D. Joubert, *Phys. Rev. B* **59**, 1758 (1999).
- [26] G. Kresse, and J. Hafner, *Phys. Rev. B* **49**, 14251 (1994).
- [27] J. P. Perdew, K. Burke, and M. Ernzerhof, *Phys. Rev. Lett.* **77**, 3865 (1996).
- [28] A. Tkatchenko, and M. Scheffler, *Phys. Rev. Lett.* **102**, 073005 (2009).
- [29] See Supplemental Material at ... for additional information from test calculations and analyses.
- [30] J.-M. Zhang, W. Zhu, Y. Zhang, D. Xiao, and Y. Yao, *Phys. Rev. Lett.* **109**, 266405 (2012).
- [31] W. Liu, D. West, L. He, Y. Xu, J. Liu, K. Wang, Y. Wang, G. van der Laan, R. Zhang, S. Zhang, and K. L. Wang, *ACS Nano* **9**, 10237 (2015).
- [32] S. Lee, K. Esfarjani, T. Luo, J. Zhou, Z. Tian, and G. Chen, *Nat. Commun.* **5**, 3525 (2014).
- [33] H. González-Herrero, J. M. Gómez-Rodríguez, P. Mallet, M. Moaied, J. J. Palacios, C. Salgado, M. M. Ugeda, J.-Y. Veuillen, F. Yndurain, and I. Brihuega, *Science* **352**, 437 (2016).
- [34] We assumed Cr dimer and trimer configurations for calculations with high Cr concentrations, as was also reported in Ref. 17.
- [35] J. Kim, and S.-H. Jhi, *Phys. Rev. B* **92**, 104405 (2015).
- [36] A. Pertsova, C. M. Canali, and A. H. MacDonald, *Phys. Rev. B* **94**, 121409 (2016).
- [37] S. Qi, Z. Qiao, X. Deng, E. D. Cubuk, H. Chen, W. Zhu, E. Kaxiras, S. B. Zhang, X. Xu, and Z. Zhang, *Phys. Rev. Lett.* **117**, 056804 (2016).